ELSEVIER

Transient confined natural convection with internal heat generation

Young Min Shim and Jae Min Hyun
Department of Mechanical Engineering, Korea Advanced Institute of Science and Technology, Taegon, South Korea

Numerical studies are conducted to describe the time-dependent adjustment of natural convection in a square cavity. A steady flow field had been established by maintaining different temperatures at the two vertical sidewalls, and this effect is represented by the external Rayleigh number Ra_E. A uniform internal heat generation, which is measured by a properly defined internal Rayleigh number Ra_I, is switched on impulsively at $t=0$. The ensuing process of settlement to final state, for large Ra_E and Ra_I, and $Pr \sim O(1)$, is depicted by solving the governing equations numerically. When the effect of internal heating is small, the major circulation cell, which has been driven by external heating, remains little affected, and this pattern is termed stage I. When Ra_I/Ra_E is moderately large, an additional oppositely directed circulation cell appears in the upper corner region of the heated sidewall, which is denoted stage II. When Ra_I/Ra_E is very large, three stages are encompassed. The qualitative flows of the first two stages correspond to those described earlier. In stage III, the whole cavity is occupied by two oppositely directed circulation cells. The final-state features are consistent with the preceding experimental visualizations for the flow dominated by internal heating effects. Time histories of the average Nusselt number on the wall are analyzed, and the overall time characterizing the global adjustment is shown to scale with $Ra_I^{-1/4}$.

Keywords: natural convection; internal heat generation; transient processes

Introduction

Natural convection in a closed square cavity, with the two vertical sidewalls maintained at different temperatures, has posed a classical configuration for benchmark testing (e.g., Davis 1983). The flow and attendant heat transfer are characterized by the externally controllable Rayleigh number $Ra_E(\equiv \beta g \Delta T L^3/\nu\kappa)$ and the Prandtl number $Pr(\equiv \nu/\kappa)$. Here, ΔT denotes the imposed temperature difference between the two sidewalls ($\Delta T \equiv T_H - T_C$), β the coefficient of volumetric expansion for a Boussinesq fluid, g the gravity, L the height of the cavity, ν and κ the kinematic viscosity and thermal diffusivity of the fluid, respectively. It has been demonstrated that for large Ra_E and $Pr \sim O(1)$, which pertain to many practical systems, the global flow is of boundary layer type. Prominent features of the convection in this side-heated square cavity have been documented extensively (e.g., Ostrach 1988; Hyun 1994).

Studies have been made of the responses of the enclosed fluid system when a differential sidewall heating and an internal heat generation are present concurrently. These efforts (Acharya and Goldstein 1985; Lee and Goldstein 1988; Kawara et al. 1994; Fusegi et al. 1992) were concerned with such technological applications as in nuclear reactors and geothermal heat extractions. The introduction of internal heat generation is represented by the internal Rayleigh number $Ra_I(\equiv g\beta QL^5/\nu\kappa k)$, in which Q denotes the rate of uniform internal heat generation, and k is the coefficient of thermal conductivity of the fluid. One significant finding of the above investigations is that, when Ra_I is substantially larger than Ra_E, the overall flow is directed downward on both the heated and cooled vertical sidewalls. Recent experimental visualizations of Kawara et al. (1994), by passing electric current through a liquid solution, classified the qualitative flow patterns in the Ra_E–Ra_I regimen diagram. For several limited cases, detailed measurements of local temperature field and heat flux were obtained, and these corroborated the depictions of the global flow character of Kawara et al.

It is notable that all of the prior works dealt with the steady-state situations in which the externally specified conditions were enforced in a time-invariant manner. Here, we probe into the transient features of confined convection when the thermal forcings are applied abruptly. Specifically, attention is directed to a sidewall-heated square cavity, in which uniform internal heat generation is started impulsively. The ensuing time-dependent process of adjustment is examined. This setup constitutes a self-standing dynamical problem from a theoretical standpoint. On the practical side, the transient approach to the final state is of relevance to the start-up (or shut-off) phase of industrial devices with internal heat generation. In this paper, numerical solutions are acquired that display the sequences of flow and thermal fields, in response to an instantaneously started internal heat generation, for large Ra_E and Ra_I with $Pr \sim O(1)$.

Address reprint requests to Prof. J. M. Hyun, Department of Mechanical Engineering, Korea Advanced Institute of Science and Technology, 373-1 Kusong-Dong, Yusong-Gu, Taejon 305-701, South Korea.

Received 27 January 1996; accepted 7 September 1996

Int. J. Heat and Fluid Flow 18: 328–333, 1997

655 Avenue of the Americas, New York, NY 10010

0142-727X/97/$17.00
PII S0142-727X(97)00027-1

In particular, we endeavor to characterize the time scale over which the global flow substantially settles to the final state by analyzing the numerical data.

Formulation

The governing Navier–Stokes equations, for a Boussinesq fluid, written in nondimensional form, are (e.g., Davis 1983):

$$\frac{\partial U}{\partial X}+\frac{\partial V}{\partial Y}=0 \tag{1}$$

$$\frac{\partial U}{\partial t}+U\frac{\partial U}{\partial X}+V\frac{\partial U}{\partial Y}=-\frac{\partial P}{\partial X}+\frac{\partial^2 U}{\partial X^2}+\frac{\partial^2 U}{\partial Y^2} \tag{2}$$

$$\frac{\partial V}{\partial t}+U\frac{\partial V}{\partial X}+V\frac{\partial V}{\partial Y}=-\frac{\partial P}{\partial Y}+\frac{\partial^2 V}{\partial X^2}+\frac{\partial^2 V}{\partial Y^2}+\frac{\mathrm{Ra}_E}{\mathrm{Pr}}\theta \tag{3}$$

$$\frac{\partial \theta}{\partial t}+U\frac{\partial \theta}{\partial X}+V\frac{\partial \theta}{\partial Y}=\frac{1}{\mathrm{Pr}}\left[\frac{\partial^2 \theta}{\partial X^2}+\frac{\partial^2 \theta}{\partial Y^2}\right]+\frac{\mathrm{Ra}_I}{\mathrm{Ra}_E\mathrm{Pr}} \tag{4}$$

in which (U,V) stand for the velocity components, t time, P pressure, θ temperature.

In the above, nondimensionalizations were made so that $(X,Y)\equiv(x^*, y^*/L)$, $(U,V)\equiv[u^*, v^*/(\nu/L)]$, $P\equiv p^*/[\rho(\nu/L)^2]$, $\theta\equiv[T-(T_H+T_C)/2]/(T_H-T_C)$, $t\equiv t^*/(L^2/\nu)$, where dimensional quantities are denoted by an asterisk. The principal dimensionless parameters explicitly appearing in the equations are the previously defined $\mathrm{Ra}_E, \mathrm{Ra}_I, \mathrm{Pr}$.

In accordance with the problem statement, the boundary conditions are (see Figure 1).

on $X=0,1$ and $Y=0,1$:

$$U=V=0$$

on $X=0$:

$$\theta=0.5$$

on $X=1$:

$$\theta=-0.5$$

on $Y=0,1$:

$$\frac{\partial \theta}{\partial Y}=0$$

The steady state, which had previously been established by the differential sidewall heating, with no internal heat generation ($Q=0$), was taken to be the initial state. At $t=0$, Q is suddenly switched on to this pre-established, sidewall-heated square cavity, and the subsequent flows are depicted.

Numerical solutions were procured by using the well-known computational procedures SIMPLER (Patankar 1980). A staggered and stretched mesh was selected, with the grid points clustered near the solid boundaries. Specifics of the numerical calculations have been elaborated in the literature. For the majority of runs, the grid network adopted was 40×40, and the time increment Δt was 10^{-5}. Extensive tests were carried out to ascertain the grid- and time interval-convergence by deploying grids 80×80 and 60×60. The variations in the computed results were shown to be smaller than 1%. Calculations were also repeated to check the present results against the published data of steady-state problems. Specific comparisons can be made between the present results depicted in Figures 2a, 3a, and 4a and the corresponding steady solutions of Davis (1983) for the sidewall-heated cavity. Also, in the limit $\mathrm{Ra}_I=0$ and $\mathrm{Ra}_E\le10^3$, the heat transfer is predominantly conductive. These explicit comparisons were previously shown in Hyun and Lee (1989). Similar endeavors are made by comparing the present results illustrated in Figures 3d and 4f and the corresponding steady solutions of Acharya and Goldstein (1985), which include internal heat generation. The outcome of such comparisons was demonstrated in Fusegi et al. (1992). These efforts provided credence to the accuracies of the present numerical model output.

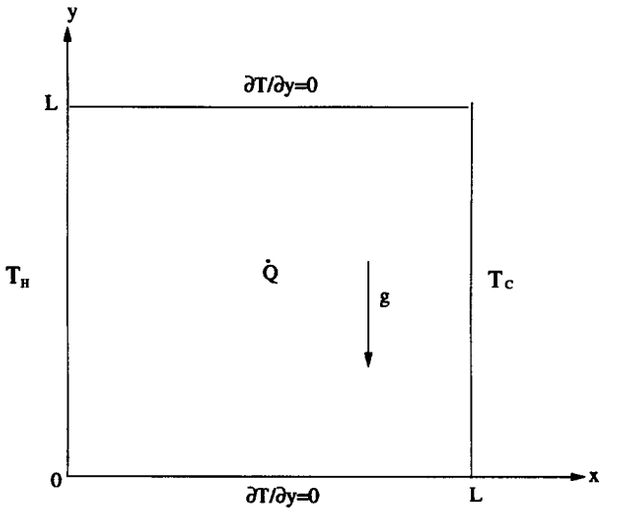

Figure 1 Schematic of the flow configuration

Results and discussion

Systematically organized computational runs were made for $\mathrm{Pr}=0.7$, covering two major parameter sets; i.e., set 1: $\mathrm{Ra}_E=10^5$, $10^5\le\mathrm{Ra}_I\le10^8$; and set 2: $10^5\le\mathrm{Ra}_E\le10^7$, $\mathrm{Ra}_I=2\times10^7$.

The selection of the above parameter sets was made to encompass the ranges of (Ra_E–Ra_I) combinations corresponding to the three distinctive final-state flow patterns, as disclosed in the regime diagram of Kawara et al. (1994). Also, the parameter sets for air $\mathrm{Pr}=0.7$ correspond closely to the steady-state results

Notation

g	gravity
Nu	local Nusselt number
Pr	Prandtl number
Q	rate of internal heat generation
Ra_E	external Rayleigh number
Ra_I	internal Rayleigh number
ΔT	temperature difference
U,V	velocity components
x,y	rectangular coordinates

of Acharya and Goldstein (1985). As asserted in Fusegi et al. (1992), the global patterns of flow and temperature fields are qualitatively similar as Pr covers the range $O(1) \leq \mathrm{Pr} \leq 10$.

First, Figure 2 shows the evolution of flow and thermal fields when the relative impact of internal heat generation is minor. The entire adjustment process, starting from the sidewall-heated established state, is dominated by the external heating. Therefore, the qualitative transient flow character is virtually unaffected. Only minor quantitative weakenings of flow at small times attributable to the introduction of Q, and their subsequent slight recoveries to the finale-state, are discernible. The flow field is characterized by the presence of a single clockwise circulation cell, which occupies much of the cavity interior. Throughout the entire curse of evolution, the temperature field deviates little from the initial-state features of the sidewall heated cavity. For the run of Figure 2, because the values of Ra_E and Ra_I are rather high, concentration of flow in thin boundary layers is evident. The flow displayed in Figure 2 was classified as Pattern I in the steady-state experiment of Kawara et al. (1994).

Next, considerations are given to the cases when the effects of external heating and internal heat generation are comparable. Figure 3 is illustrative of the sequences of flow and thermal fields for such cases. Immediately after the switch on of Q, the flow field is still mostly governed by the pre-existing external heating. Throughout the cavity interior, a single clockwise circulation cell is visible. The cavity interior region, apart from the sidewall boundary layers, is substantially stratified, with a near-liner vertical temperature distribution. As time elapses, the impact of internal heat generation provides an aiding (opposing) buoyancy effect to the fluid in the vicinity of the cold (heat) sidewall. The sinking (rising) motion in the boundary layer on the cold (hot) sidewall is, therefore, enhanced (hindered). In the bulk of the interior, generally rising motions are induced because of the presence of internal heat generation. At moderate times (see Figure 3b), caused by this differential buoyancy effect, flows are intensified near the bottom part of the cold sidewall. In the upper corner region of the hot sidewall, the additional negative buoyancy arising from Q begins to produce a vertically downward motion. As time progresses toward the final state, a small counterclockwise circulation cell in this corner is evident. As can be noted by inspecting the value of $\Psi_{\max}$, local intensifications of flows are seen as the final state is approached. The large-time flow behavior (see Figure 3d) is characteristic of Pattern II, which was portrayed by Kawara et al. (1994). The evolution of the isotherms is of interest. At small times, because of the dominance of external heating, the isotherms are diagonally symmetric with respect to the cavity center. At moderate times, this point symmetry is destroyed as a consequence of the accumulated effect of Q. At large times, isotherms are nearly vertical and clustered in the vicinity of the cold wall, in particular, in the upper corner region. Near the hot sidewall, the isotherm of T_H divides the isotherms into two groups, one attached to the top and the other attached to the bottom horizontal wall, respectively. The cumulative effect of Q brings forth an increase of the overall thermal energy in the cavity. As shown in Figure 3d, at large times, the maximum temperature in the cavity is appreciably higher than T_H.

The evolution of flow, when the effect of internal heat generation is dominant, is depicted in Figure 4. At very early times, the flow is still under the influence of external heating and, as expected, a single clockwise circulating cell occupies much of the cavity. In the intermediate stage, the impact of Q begins to be felt, and an additional differential buoyancy is produced. As is evident in Figure 4c and d, a small-sized, counterclockwise circulation emerges in the upper corner of the heated sidewall. This is similar to the previously mentioned Pattern II of Kawara et al. (1994). As time passes, the relative effect of internal heat generation outweighs that of external heating. In the central portion of the cavity interior, generally rising motions prevail. Near the hot wall, the sinking motion arising from the negative buoyancy attributable to Q is appreciable. In the vicinity of the cold wall, the sinking motion is augmented. In the last stage settling into the final state, the whole cavity is occupied by two circulating cells; i.e., a counterclockwise (clockwise) cell near the hot (cold) wall side, respectively. This is characteristic of Pattern III, as visualized in the experiment of Kawara et al. In summary, when

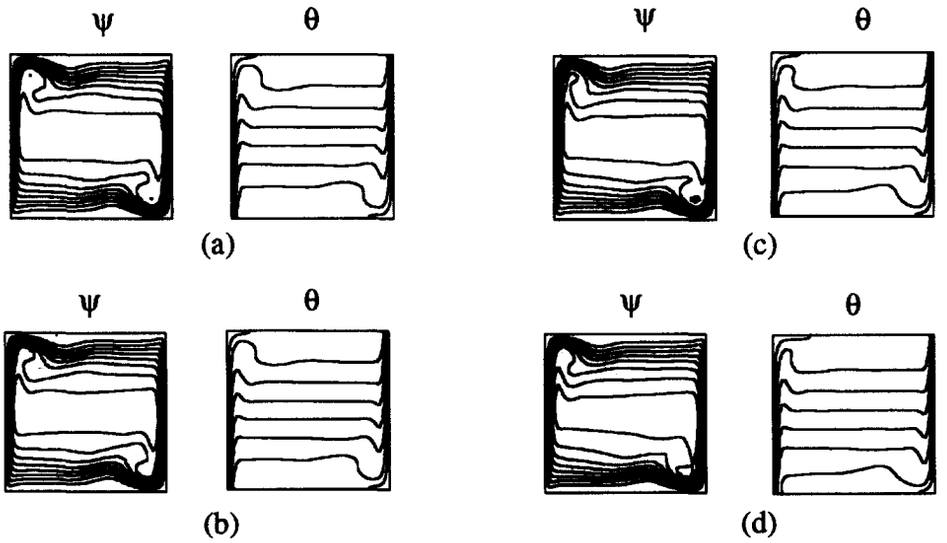

Figure 2 Sequential plots of stream function (ψ) and isotherms (θ); $\mathrm{Ra}_E = 10^7$, $\mathrm{Ra}_I = 2 \times 10^7$; (a) $t=0$, $\psi_{\max} = 2.23 \times 10^{-4}$, $\psi_{\min} = -43.3$, $\theta_{\max} = 0.50$; (b) $t=0.0001$, $\psi_{\max} = 3.08 \times 10^{-2}$, $\psi_{\min} = -41.8$, $\theta_{\max} = 0.50$; (c) $t=0.01$, $\psi_{\max} = 4.33 \times 10^{-4}$, $\psi_{\min} = -42.7$, $\theta_{\max} = 0.50$; (d) $t=0.1$, $\psi_{\max} = 1.54 \times 10^{-5}$, $\psi_{\min} = -43.3$, $\theta_{\max} = 0.50$

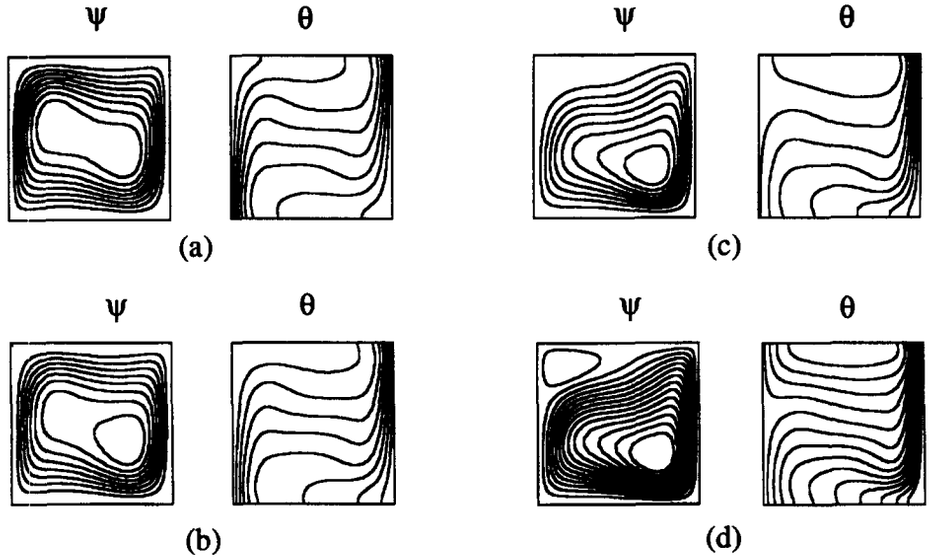

Figure 3 Sequential plots of stream function (ψ) and isotherms (θ); $Ra_E=10^5$, $Ra_I=10^6$; (a) $t=0$, $\psi_{max}=6.18\times10^{-7}$, $\psi_{min}=-13.7$, $\theta_{max}=0.50$; (b) $t=0.01$, $\psi_{max}=3.85\times10^{-4}$, $\psi_{min}=-14.8$, $\theta_{max}=0.51$; (c) $t=0.05$, $\psi_{max}=4.34\times10^{-1}$, $\psi_{min}=-16.8$, $\theta_{max}=0.75$; (d) $t=0.1$, $\psi_{max}=1.56$, $\psi_{min}=-17.0$, $\theta_{max}=0.87$

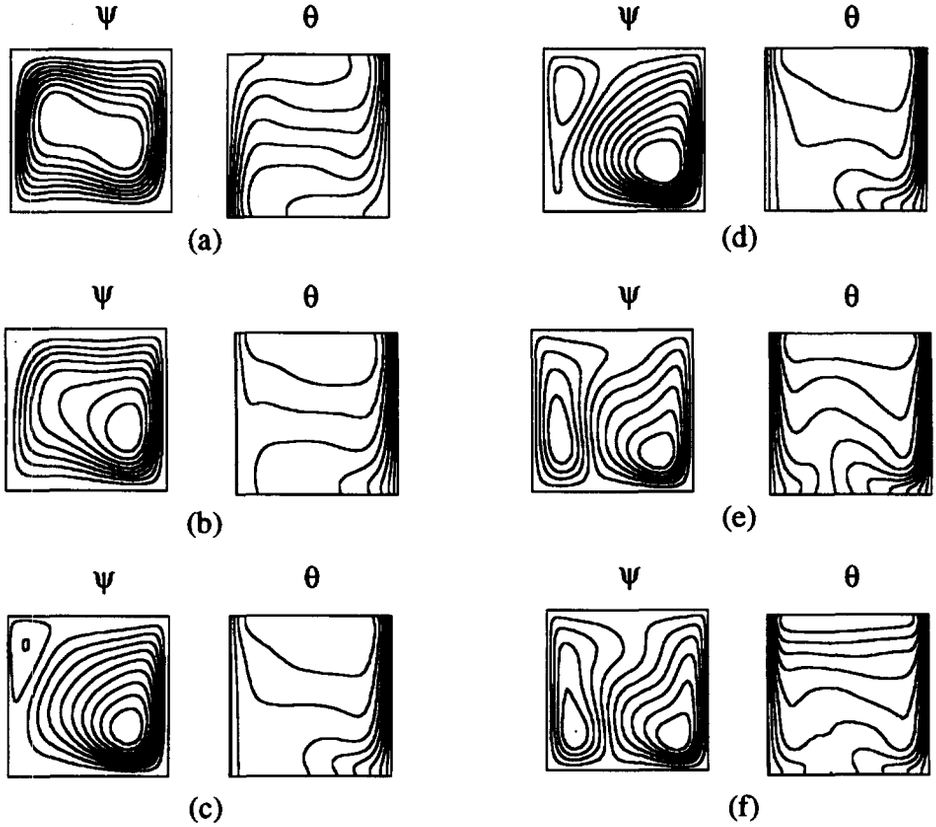

Figure 4 Sequential plots of stream function (ψ) and isotherms (θ); $Ra_E=10^5$, $Ra_I=10^7$; (a) $t=0.0001$, $\psi_{max}=4.11\times10^{-5}$, $\psi_{min}=-13.7$, $\theta_{max}=0.50$; (b) $t=0.005$, $\psi_{max}=4.73\times10^{-1}$, $\psi_{min}=-17.1$, $\theta_{max}=1.05$; (c) $t=0.008$, $\psi_{max}=2.69$, $\psi_{min}=-22.0$, $\theta_{max}=1.44$; (d) $t=0.01$, $\psi_{max}=5.96$, $\psi_{min}=-24.0$, $\theta_{max}=1.71$; (e) $t=0.02$, $\psi_{max}=16.4$, $\psi_{min}=-24.5$, $\theta_{max}=2.95$; (f) $t=0.1$, $\psi_{max}=17.2$, $\psi_{min}=-24.1$, $\theta_{max}=5.54$

the effect of internal heat generation is dominant, the flow undergoes the three stages, passing through Patterns I, II, and III of Kawara et al. The evolution of the associated thermal fields, as exhibited in Figure 4, is also revealing. In the first stage, the temperature distribution, shown in Figure 4a, is typical of the conventional sidewall-heated cavity. With the introduction of Q, the crowding (thinning out) of the isotherms in the vicinity of the cold (hot) sidewall is apparent, as in Figure 4b. In the completion of the second stage (see Figure 4d), the near-linear temperature profiles in the cavity interior are broken. In the upper part of the cavity interior, temperature distributions tend to become horizontally uniform and vertically linear. However, in the bottom part of the cavity interior, in line with the emergence of two circulation cells of comparable magnitude, the isotherms are divided into two groups. In the last phase of the adjustment process (Figure 4f), the velocity and temperature fields display features that are characteristic of the cavity flow under dominant influence of internal heat generation. The total thermal energy in the cavity is on the increase during the adjustment process. This is reflected in the values of maximum temperature in the system, as time progresses. As the final state is approached, $T_{\max}$ is substantially larger than T_H.

It is of interest to gauge the time over which the overall adjustment is substantially accomplished. For this purpose, it is useful to plot the time histories of the average Nusselt number on the hot sidewall, which is defined as

$$\overline{\mathrm{Nu}} = \int_0^1 \left(\frac{\partial \theta}{\partial X} \right)_{X=0} \mathrm{d}Y$$

The objective here is to characterize the principal time scale for the flows to settle from the impulsive start to the final state. Based on the numerical data, the computed $\overline{\mathrm{Nu}}$ traces are exhibited in Figure 5. The four frames illustrated in Figure 5 encompass the situations whose final states lead to the three specific patterns describes earlier. When the effect of Q is relatively minor (see Figure 5a), the overall values of $\overline{\mathrm{Nu}}$ are moderate, and the decay of $\overline{\mathrm{Nu}}$ with time is mild. Obviously, because the flow is little affected by Q, the temporal variation of $\overline{\mathrm{Nu}}$ is expectedly small. In Figure 5b, the relative importance of Q is comparable to that of external heating, and the total heat transfer on the hot wall shows a steeper decay with time. When the flow is dominated by Q, as seen in Figure 5c and d, the total heat transfer on the hot wall is directed go the environment (note that $\overline{\mathrm{Nu}}$ is negative), and the heat transfer rate increases substantially as $\mathrm{Ra}_I/\mathrm{Ra}_E$ becomes large. Inspecting these time traces of $\overline{\mathrm{Nu}}$, a curve fitting is attempted in the exponential decay form; i.e., $\overline{\mathrm{Nu}} \sim A_0 + A_1[1 - \exp(-t/t_c)]$. The time constant t_c implies that the adjustment to the final state is approximately 63% completed. After considerable numerical effort, it is found that t_c is closely scaled with $\mathrm{Ra}_I^{-1/4}$. This may be explained in physical terms. When the impact of Q is weak, such as in Figure 5a, the numerical values of Ra_E and Ra_I are of the same order of magnitude. In this case, the flow adjustment is controlled by the external heating, and the relevant time scale for the global process has been established to be $O(\mathrm{Ra}_E^{-1/4})$, which is comparable to $O(\mathrm{Ra}_I^{-1/4})$. When the influence of Q is appreciable or overwhelming, the time-dependent motions arise principally because of the switch on of the internal heat generation, as demonstrated in Figures 3 and 4. For these cases, the evolution of flow is largely controlled by the accumulated effect of internal heating. The establishment of the boundary layers, which is dominated by internal heat generation, is crucial to drive the counter-

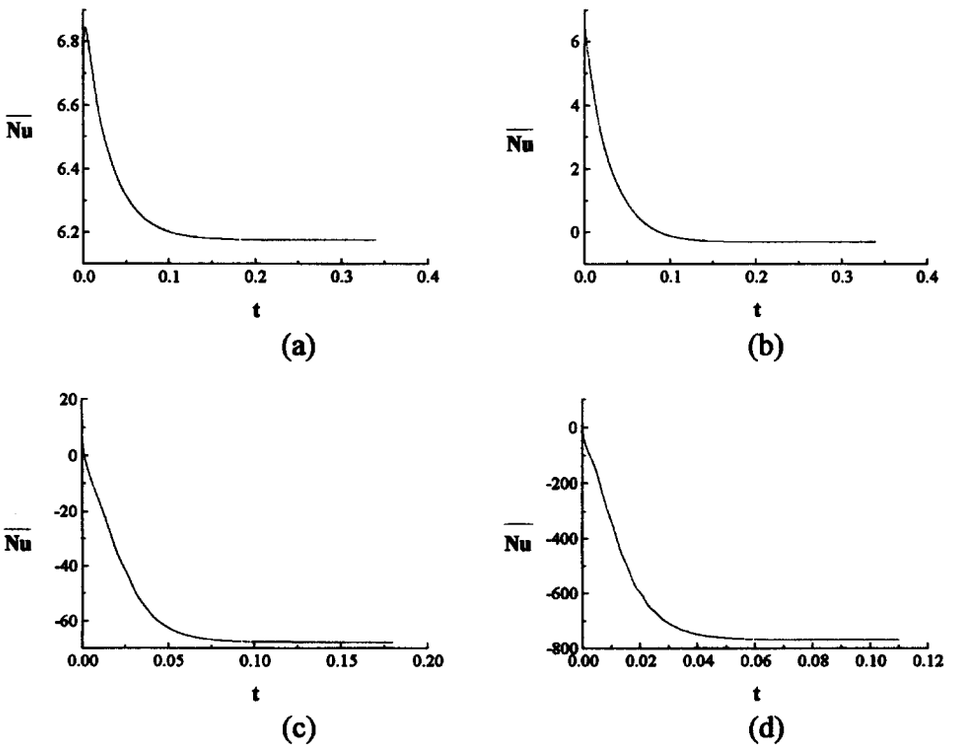

Figure 5 Temporal variation of average Nusselt number on the hot sidewall; curve fitting in the form of $\overline{\mathrm{Nu}} = A_0 - A_1[1 - \exp(-t/t_c)]$ is performed; (a) $\mathrm{Ra}_E = 10^5$, $\mathrm{Ra}_I = 10^5$, $A_0 = 6.62$, $A_1 = 0.45$, $t_c = 0.049$; (b) $\mathrm{Ra}_E = 10^5$, $\mathrm{Ra}_I = 10^6$, $A_0 = 7.44$, $A_1 = 1.00$, $t_c = 0.025$; (c) $\mathrm{Ra}_E = 10^5$, $\mathrm{Ra}_I = 10^7$, $A_0 = 7.59$, $A_1 = 76.1$, $t_c = 0.022$; (d) $\mathrm{Ra}_E = 10^5$, $\mathrm{Ra}_I = 10^8$, $A_0 = 42.8$, $A_1 = 820$, $t_c = 0.013$

clockwise circulation cell. In the final state, the thickness of boundary layer is given as $Ra_I^{-1/4}$. Therefore, in order to grow to this thickness, the time needed would be $Ra_I^{-1/4}$, using the present nondimensionalization schemes. The numerical fittings, which point to the time scale $O(Ra_I^{-1/4})$, are consistent with the above qualitative physical reasoning.

Conclusion

Numerical results indicate that when Ra_I/Ra_E is substantially large, the evolution encompasses the three stages. The first stage is typified by a single cell. In the second stage, an additional small oppositely directed cell appears in the upper corner region of the hot sidewall. In the last stage settling to the final state, the whole cavity is occupied by two circulation cells. The large-time behavior is consistent with Pattern III of the steady-state visualization of Kawara et al. (1994). In conjunction with the flow development, the temperature field undergoes an evolutionary process leading to the final state.

Numerical data for the evolution of the average Nusselt number of the hot sidewall are analyzed. When the impact of internal heat generation is dominant, the global flow adjustment is substantially achieved over the time that is scaled with $O(Ra_I^{-1/4})$.

References

Acharya, S. and Goldstein, R. J. 1985. Natural convection in an externally heated vertical or inclined square box containing internal energy sources. *J. Heat Transfer*, **107**, 855–866

deVahl Davis, G. 1983. Natural convection of air in a square cavity: A benchmark numerical solution. *Int. J. Num. Meth. Fluids*, **3**, 249–264

Fusegi, T., Hyun, J. M. and Kuwahara, K. 1992. Natural convection in a differentially heated square cavity with internal heat generation. *Num. Heat Transfer*, **21** 215–229

Hyun, J. M. 1994. Unsteady buoyant convection in an enclosure. *Adv. Heat Transfer*, **24**, 277–230

Hyun, J. M. and Lee, J. W. 1989. Numerical solution for transient natural convection in a square cavity with different sidewall temperatures. *Int. J. Heat Fluid Flow*, **10**, 146–151

Kawara, Z. Takahashi, O. Serizawa, A. and Michiyoshi, I. 1994. Natural convection in a confined regime with internal heating. *Proc. 1st Symposium on Heat Mass Transfer*, (Kansai Branch of the Heat Transfer Soc. Japan, Nov. 28–29), 153–158

Lee, J. H. and Goldstein, R. J. 1988. Experimental study on natural convection heat transfer in an inclined square enclosure containing internal energy sources. *J. Heat Transfer*, **110**, 345–349

Ostrach, S. 1988. Natural convection in enclosures. *J. Heat Transfer* **110**, 1175–1190

Patankar, S. V. 1980. *Numerical Heat Transfer and Fluid Flow*. Hemisphere, Bristol, PA